




# Compact ACS-fed MIMO antenna with dual-band notch characteristics for UWB applications

Zhongyuan Lu<sup>1</sup> , Han Lin<sup>1</sup>, Zhonggen Wang<sup>1</sup>, Wenyan Nie<sup>2</sup> and Weidong Mu<sup>1</sup>

<sup>1</sup>School of Electrical and Information Engineering, Anhui University of Science and Technology, Huainan, China and <sup>2</sup>School of Mechanical and Electrical Engineering, Huainan Normal University, Huainan, China

## Research Paper

**Cite this article:** Lu Z, Lin H, Wang Z, Nie W, Mu W (2024) Compact ACS-fed MIMO antenna with dual-band notch characteristics for UWB applications. *International Journal of Microwave and Wireless Technologies* **16**(3), 478–486. <https://doi.org/10.1017/S1759078723001277>

Received: 04 April 2023  
Revised: 18 October 2023  
Accepted: 20 October 2023

**Keywords:**  
asymmetric coplanar strip; diversity performance; dual-band notch characteristics; MIMO antenna

**Corresponding author:** Han Lin;  
Email: [hanlin@aust.edu.cn](mailto:hanlin@aust.edu.cn)

### Abstract

An ultra-wideband (UWB) and compact-size four-port multiple input multiple output (MIMO) antenna with a footprint of 34 mm × 34 mm fed by an asymmetric coplanar strip (ACS) is investigated. The proposed antenna is composed of four orthogonally placed identical modified elliptical-shaped radiators and achieves an impedance bandwidth of 3.4–12.2 GHz. By etching two inverted L-shaped slots in the radiator element, WLAN band and X-band are rejected in the operating communication range. Because of the usage of a meander line decoupler, the isolation enhancement at the 8–12 GHz band is achieved and the isolation is more than 18 dB for most of the UWB range. The performance of the proposed antenna is studied in terms of isolation between each port, radiation pattern, current distribution, gain, envelope correlation coefficient, diversity gain, and total active reflection coefficient. The compact size and reduced complexity make the proposed design highly suitable for portable devices.

### Introduction

Since ultra-wideband (UWB) technology has the advantages of high-speed data transmission and ease of manufacturing at low power. UWB technology has acquired considerable popularity in the current communication era. However, the problems of signal fading in a multipath environment and the limitation of power density will negatively impact the performance of UWB system, which limit the range of communication of UWB system. Thus, in order to increase channel capacity, reduce latency, and improve communication quality and resilience, multiple input multiple output (MIMO) technology has been adopted in combination with UWB technology. Moreover, miniaturization of the antenna facilitates the integration of the antenna in the circuit system. In terms of the miniaturization design of the antenna, conventional Co-Planar Waveguide (CPW) feed methods occupy most of the antenna size. Similar to the CPW feeding method, the asymmetric coplanar strip (ACS) feeding method only has one lateral ground strip. Since all ground wires are on the upper surface of the coplanar waveguide structure, other devices can be easily connected in series or in parallel, thus eliminating the need for contact holes and effectively reducing costs. So the ACS-fed antenna has the advantages of uniplanar nature with compactness [1–3].

Furthermore, the existence of mutual coupling between the antenna elements that are placed closely cannot be ignored. Over the past few years, there has been a proliferation of research into optimizing the mutual coupling of antennas [4–6]. In the study by Luo et al. [7], a T-shaped slot is etched to increase the distance between the two input ports and two defected ground structures are utilized to develop a high isolation of the compact MIMO antenna. The low mutual coupling can also be realized by using a neutralization line into antenna elements, thereby avoiding the need for extra space [8, 9]. Besides, a metasurface-based decoupling method is provided in the study by Liu et al. [10], which ensures the isolation of more than 25 dB at both 2.5–2.7 GHz and 3.4–3.6 GHz bands. Wang et al. [11] proposed a fence-type decoupling structure on the other side of the radiating elements, with two L-shaped stubs loaded on the same side of the radiating elements to enhance the isolation. The fence-type decoupling structure plays a role in extending the current path, thus the isolation is more than 25 dB in the UWB band. Lin et al. [12] introduced a carbon black film to improve the isolation in the MIMO system. The carbon black film is coated on the feed line of the MIMO antenna. In the study by Zhou et al. [13], two H-shaped slots and two split-ring resonator slots are etched on the ground plane, achieving a promising isolation between two adjacent input ports.

In addition, within the defined UWB range, various narrowband communication systems, including wireless local area networks (WLAN) and X-satellite communication bands, may bring electromagnetic interference that affects the performance of UWB antennas. Therefore, it is of great significance to study antennas with notch characteristics to suppress specified interference frequency bands [14, 15]. In the study by Kapure and Rathod [16], a single electromagnetic

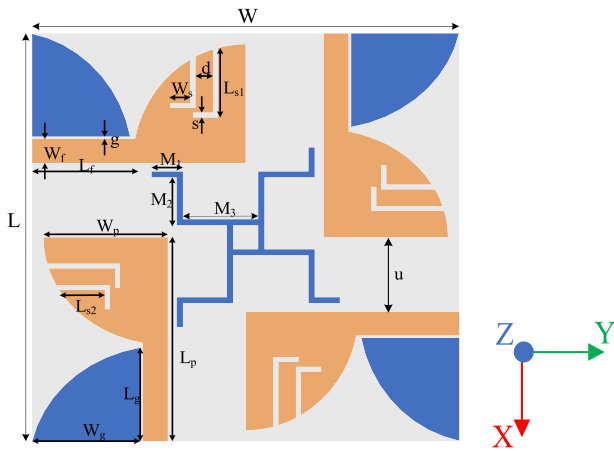


**Figure 1.** The top view of the geometry of the proposed four-port ACS-fed MIMO antenna.

**Table 1.** Optimized dimensions of the proposed four-port ACS-fed MIMO antenna

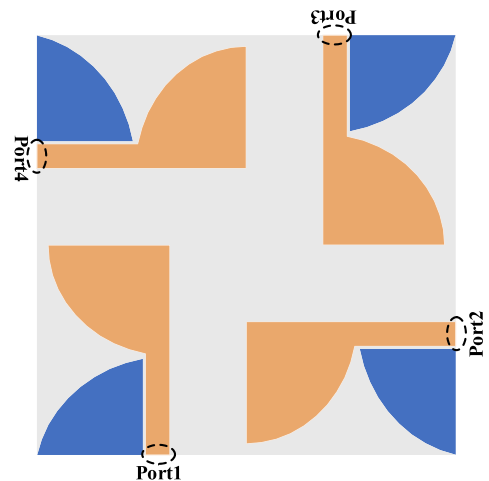
L	W	L <sub>p</sub>	W <sub>p</sub>	L <sub>g</sub>	W <sub>g</sub>
34	34	17	9.9	7.8	8.6
L <sub>f</sub>	W <sub>f</sub>	L <sub>s1</sub>	L <sub>s2</sub>	W <sub>s</sub>	s
8.2	2	5.8	3.8	2	0.4
M <sub>1</sub>	M <sub>2</sub>	M <sub>3</sub>	d	g	u
2	4	6	1.4	0.2	6.2

bandgap structure is utilized to suppress WiMAX, WLAN, and uplink X-bands. In the study by Chakraborty et al. [17], WiMAX, upper WLAN, and lower WLAN bands are suppressed by etching three U-shaped slots on the radiating element and ground plane, while X-band is suppressed by introducing a split-ring resonator. Similar to this manuscript is the notch method in the study by You et al. [18], where two C-shaped slots are engraved to reject WLAN and X-band.

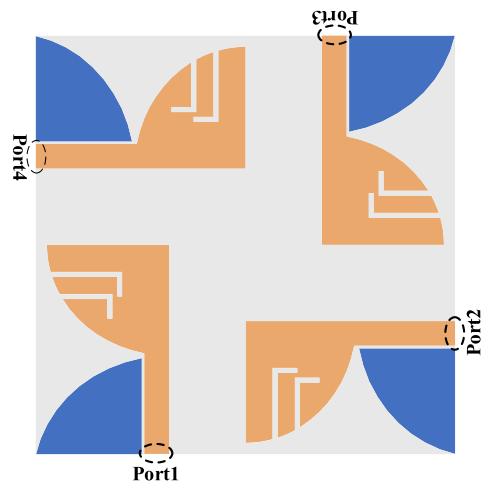
In this article, a compact four-port antenna array with WLAN and X-band rejection capabilities is proposed. The novelty of the proposed antenna lies in using ACS miniaturizing technique along with the MIMO orthogonal configuration, benefiting from the advantages of each. Different from the decoupling structures in the study by Yang and Zhou [19], a novel decoupling structure, consisting of four rotating meander line stubs, is introduced to enhance isolation between antenna elements. The efficacious and simple isolator design achieves not only a wider impedance bandwidth but also the isolation of more than 18 dB throughout the entire frequency range. The proposed antenna is applicable for UWB communication systems that require shielding WLAN and X-satellite bands.

**Antenna design**

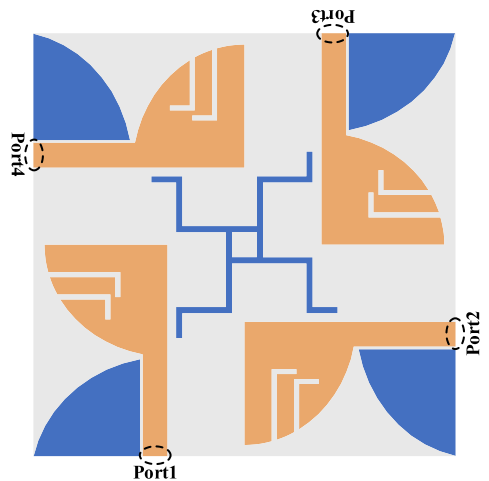
The geometry of the proposed MIMO antenna is shown in Fig. 1. Four orthogonally placed identical radiating elements and ground planes are printed on the upper surface of the 1.6 mm-thick flame retardant-4 epoxy substrate ( $\tan\delta = 0.02$ ) with a relative permittivity of 4.4. A single radiating element excited by the ACS is composed of a quarter-elliptical patch in which two



(a)



(b)



(c)

**Figure 2.** Three configurations derived from the evolutionary process of the proposed MIMO antenna: (a) Ant.1, (b) Ant.2, (c) Ant.3.

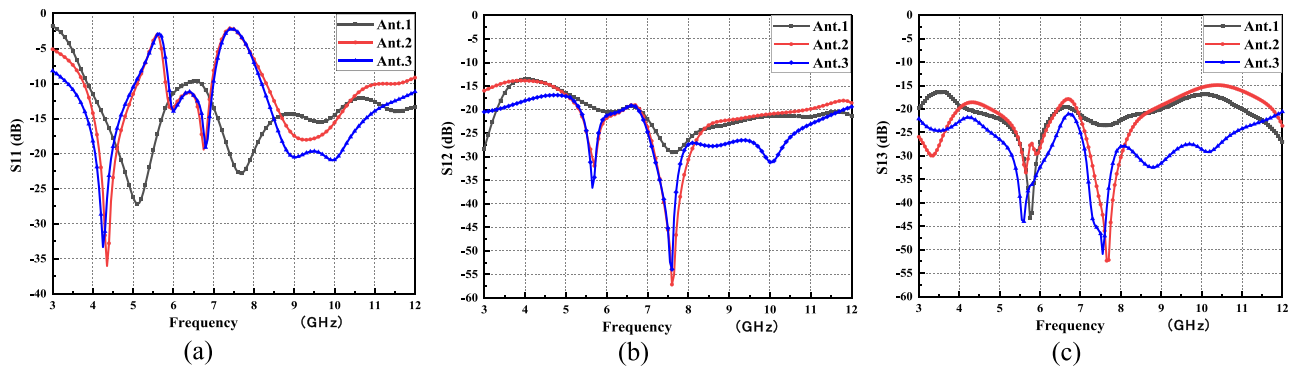


**Figure 3.** Comparison of S parameters of each proposed antennas: (a) S11, (b) S12, and (c) S13.

L-shaped slots are etched on its surface to achieve dual-band notch characteristics. The finally optimized values of the proposed antenna are shown in Table 1.

To clarify the process of the proposed antenna design, three forms of the proposed MIMO antenna are shown in Fig. 2. The results of the comparison of S parameters of three forms of MIMO antenna are shown in Fig. 3.

On the basis of Ant.1, a pair of L-shaped slits are etched side by side of each radiating element. This modification changes the effective current path and impedance bandwidth. Simultaneously, the lowest resonant frequency of the antenna shifts to a lower frequency, and the frequency range of 5.1–5.8 GHz and 7.0–8.1 GHz are suppressed. Furthermore, the coupling between adjacent elements is significantly reduced at 5.2–6.1 GHz, while the coupling between opposite elements is significantly reduced at 6.8–8.4 GHz. The total length of the L-shaped slot is designed to fulfill the following equations:

$$L_1 = L_{s1} + W, \quad (1)$$

$$L_2 = L_{s2} + W, \quad (2)$$

$$L_{slot} = \frac{c}{4f_{notch} \sqrt{(\epsilon_r + 1)/2}}. \quad (3)$$

where  $L_1$  is the total length of the upper L-shaped slot,  $L_2$  is the total length of the lower L-shaped slot,  $L_{slot}$  is the total length of the L-shaped slot,  $c$  is the speed of light,  $f_{notch}$  is the desired frequency of the notch band, and  $\epsilon_r$  is the relative permittivity of the substrate.

To further optimize the isolation performance between the antenna elements, Ant.3 introduces a meander line isolator to reduce the coupling between adjacent elements at 3–4.6 GHz and 8.2–12 GHz. The end branches of the meander line are coupled with the radiation elements, ensuring isolation greater than 18 dB over the entire operating band and extending the impedance bandwidth effectively. More than this, due to the existence of the isolator, isolation between opposite elements is greater than 20 dB over the entire bandwidth.

Figure 4 illustrates the effect of the variations in parameters on antenna performance. As “ $L_{s1}$ ” increases, the frequency range of the first notch band changes from 5.1–5.8 GHz to 4.6–5.6 GHz. Conversely, as “ $L_{s2}$ ” decreases, the frequency range of the second notch band changes from 7.0–8.1 GHz to 7.4–8.3 GHz. It indicates that the length of the L-shaped slot can be flexibly adjusted according to the frequency of the notch band. In addition, the decrease in

“ $M_2$ ” means that the distance between the isolator and the radiation elements increases. In this case, it is difficult for the isolator to absorb the current on the radiator, resulting in enhanced coupling between antenna elements.

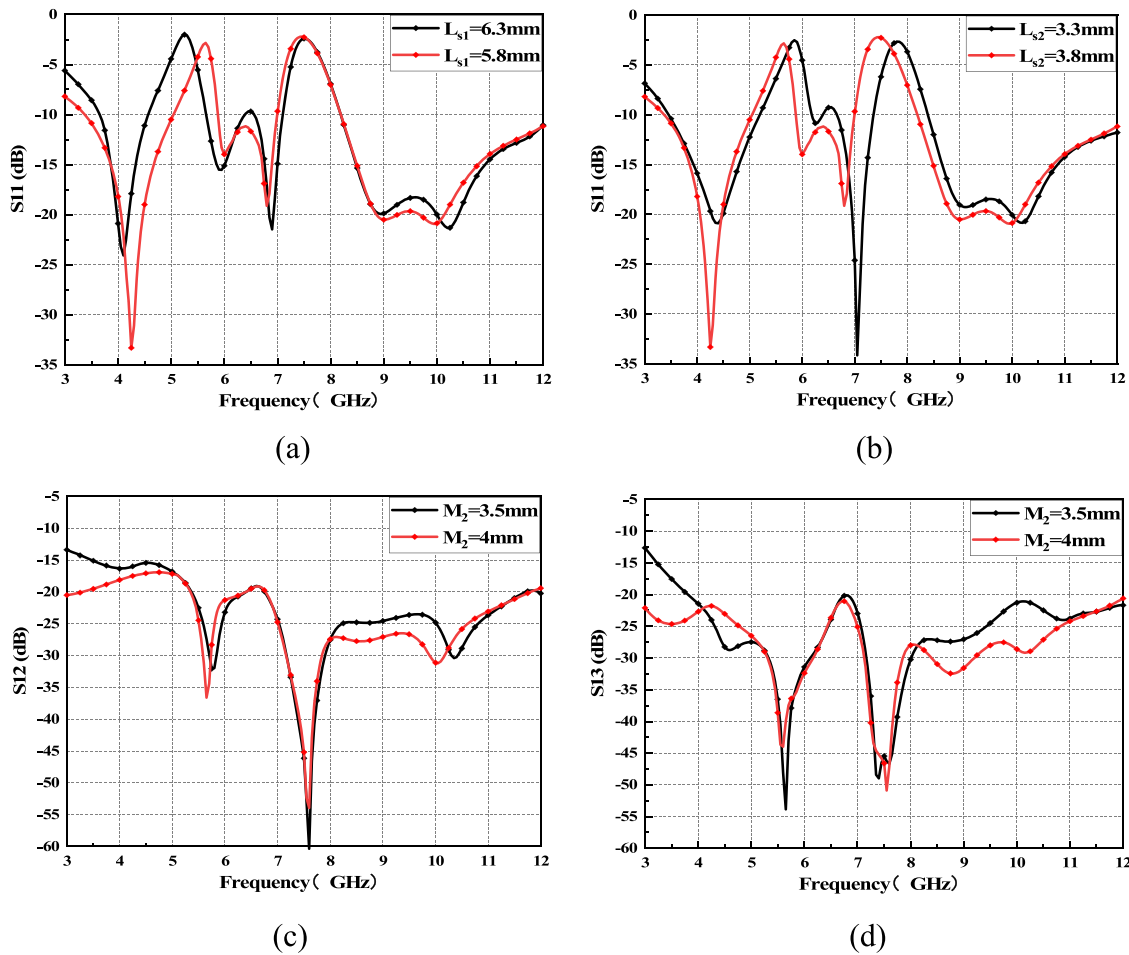
The effect of introducing an isolator can be observed by comparing Fig. 5(a) and (c), (b) and (d). It is worth noting that the antennas in Fig. 5(a–d) only activated port 1. The frequencies chosen are those where the differences in S parameters are relatively clear. When port 1 is activated, ports 2, 3, and 4 are terminated with matched load. The current is mainly distributed to the radiating element 1 and the meander line of its adjacent isolator, while there is almost no current distribution on the surface of ports 2, 3, and 4. It can be seen that the isolator absorbs part of the current and plays a decoupling role.

Figure 6(a) and (b) shows the effect of the etched double L-shaped slots side by side on the antenna current distribution, where 5.6 GHz and 7.4 GHz are the center notch frequencies of the proposed antenna. The current is mainly concentrated around the upper L-shaped slot at 5.6 GHz. Similarly, at 7.4 GHz, the surface current is mainly concentrated around the lower L-shaped slot, indicating the significant effect of the notch structure.

## Experimental results

To validate the accuracy of the simulated results, an experimental prototype of the MIMO antenna is fabricated. An Agilent E5080A network analyzer and a Satimo Starlab near-field measurement system are used to test the performance characteristics of the proposed antenna. Figure 7 provides the photograph of the antenna prototype and pattern measurement environment. Figure 8 illustrates the result of the comparison of measured and simulated S parameters. There are some differences between the simulation results and the measurements results, which are caused by the unavoidable wear and tear during the production and welding processes of the antenna and the fluctuation of the relative dielectric constant of FR4 dielectric material in the high-frequency range.

In this section, the radiation patterns of the proposed MIMO antenna are investigated. As Fig. 9 illustrates, the simulated and measured two-dimensional radiation patterns of the antenna in free space along the E-plane (xz plane) and H-plane (yz plane) at sample frequencies of 4.2, 6.8, and 9.2 GHz, respectively, were given, which represent low, intermediate, and high frequencies within UWB bandwidth. The radiation patterns are measured when port 1 is activated and the other ports are terminated by the



**Figure 4.** (a) Effect of varying “ $L_{s1}$ ” parameter of L-shaped slot on S11. (b) Effect of varying “ $L_{s2}$ ” parameter of L-shaped slot on S11. (c) Effect of varying “ $M_2$ ” parameter of the meander line isolator on S12. (d) Effect of varying “ $M_2$ ” parameter of the meander line isolator on S13.

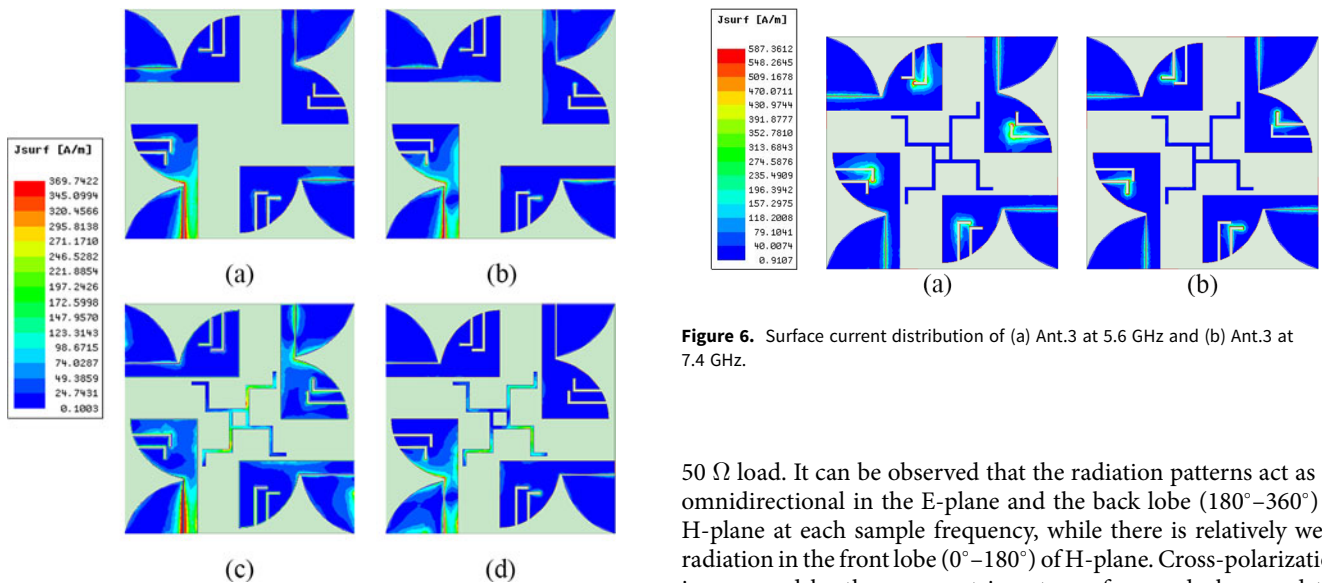
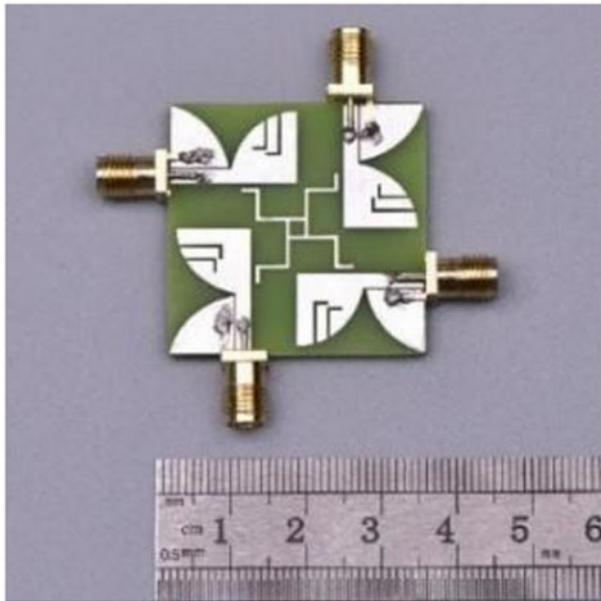


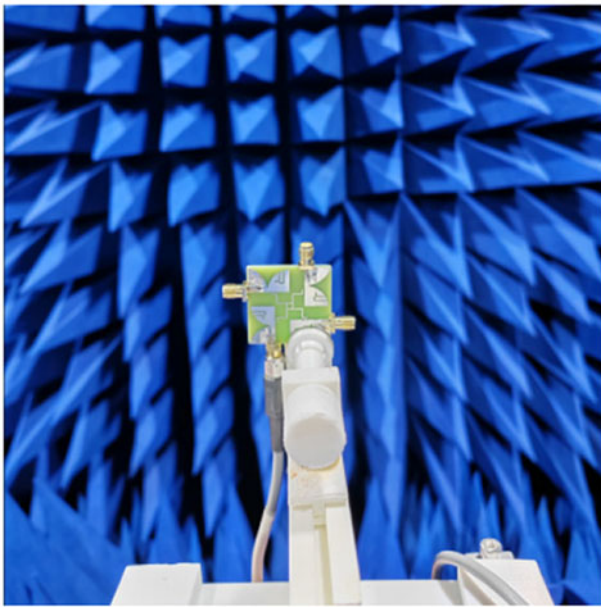
**Figure 5.** Surface current distribution of (a) Ant.2 at 3.0 GHz, (b) Ant.2 at 10.1 GHz, (c) Ant.3 at 3.0 GHz, and (d) Ant.3 at 10.1 GHz.

**Figure 6.** Surface current distribution of (a) Ant.3 at 5.6 GHz and (b) Ant.3 at 7.4 GHz.

50  $\Omega$  load. It can be observed that the radiation patterns act as an omnidirectional in the E-plane and the back lobe ( $180^\circ$ – $360^\circ$ ) of H-plane at each sample frequency, while there is relatively weak radiation in the front lobe ( $0^\circ$ – $180^\circ$ ) of H-plane. Cross-polarization is governed by the asymmetric nature of ground plane and the feeding structure, which induces the orthogonal modes that are perpendicular to the surface of the radiator. The co-polarization to



(a)

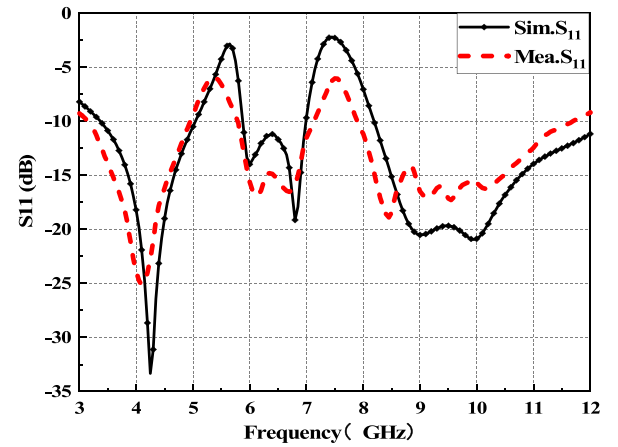


(b)

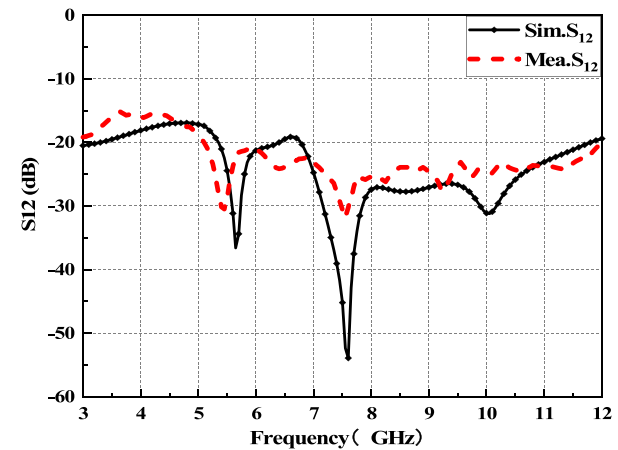
**Figure 7.** (a) Fabricated prototype of the four-port MIMO antenna. (b) Pattern measurements in anechoic chamber.

cross-polarization ratio is maintained as  $-16$  dB at  $4.2$  GHz,  $-17$  dB at  $6.8$  GHz, and  $-21$  dB at  $9.2$  GHz. Essentially, it can be assumed that the antenna can transmit and receive signals well in various wireless networks.

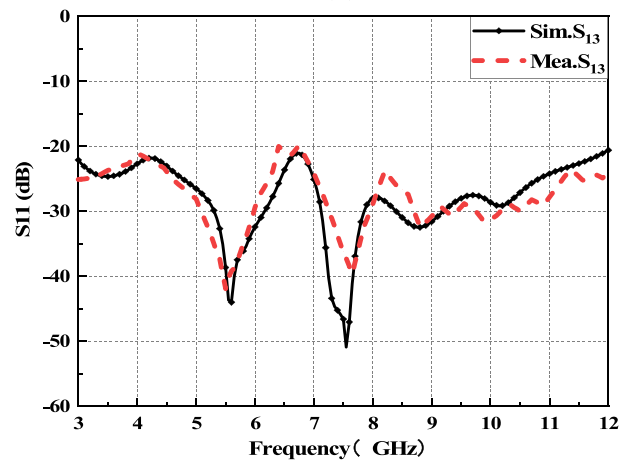
Figure 10 provides the peak gain and radiation efficiency results of the proposed MIMO antenna. The efficiency curves indicate that the proposed antenna has the ability to radiate most of its energy within the operating frequency band, but at notch frequencies, due



(a)



(b)



(c)

**Figure 8.** Comparison of measured and simulated results: (a) S11, (b) S12, and (c) S13.

to impedance mismatch, the energy of the signal source forms a standing wave on the transmission line, resulting in incomplete absorption of energy, so the efficiency has a sharp decline at notch frequencies. Similarly, the peak gain varies from  $2.6$  to  $5.9$  dBi over the entire operating frequency range, and it drops to  $-3.8$  dBi in



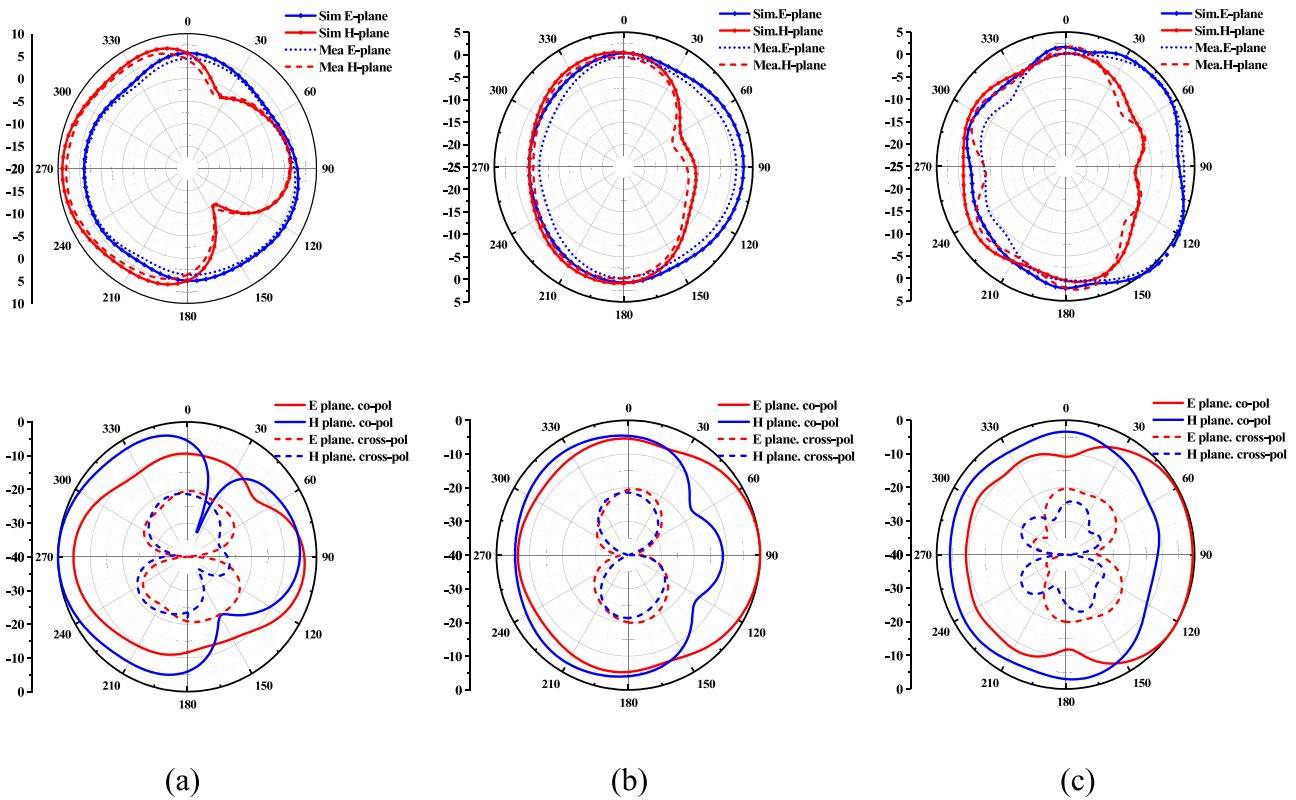


Figure 9. Radiation patterns in the E-plane and H-plane at the frequencies of (a) 4.2 GHz, (b) 6.8 GHz, and (c) 9.2 GHz.

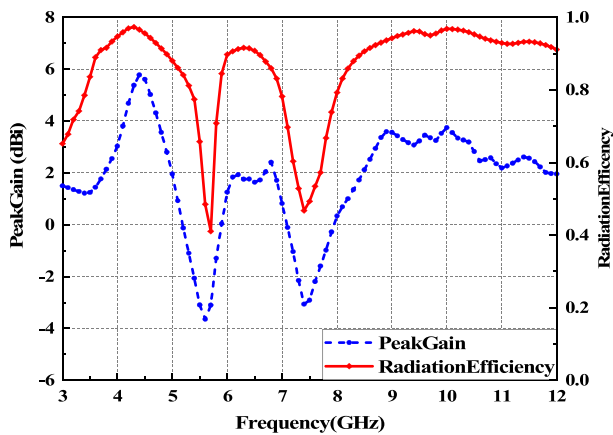


Figure 10. Peak gain and radiation efficiency of the proposed ACS MIMO antenna.

the rejected band. In general, the proposed antenna possesses an acceptable gain and radiation efficiency.

Another important parameter used to evaluate the performance of UWB antennas is group delay, which is the time delay generated by the input signal when traveling through the antenna. The time-domain test setup is shown in Fig. 11. During the measurement process, two identical prototypes are placed face to face at a distance of 25 cm. As can be seen in Fig. 12, the group delay of the proposed antenna remains nearly constant over the entire UWB frequency spectrum, except for notch bands. Ideally, the group delay of the antenna must remain constant while the phase is strictly linear. Thus, the proposed antenna possesses good pulse handling capability and linear phase.

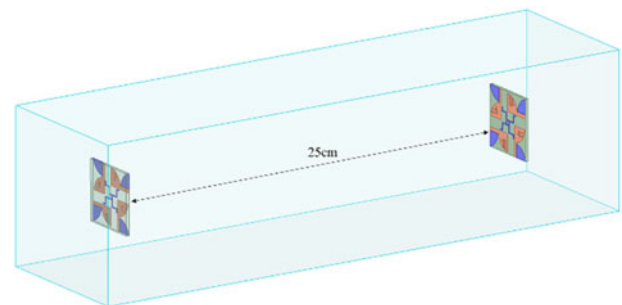


Figure 11. Time-domain analysis test setup.

### MIMO antenna performance

To verify the capability of the proposed antenna for MIMO applications, performance evaluation parameters such as envelope correlation coefficient (ECC), diversity gain (DG), and total active reflection coefficient (TARC) are discussed.

### Envelope correlation coefficient

ECC is a metric that describes the degree to which communication channels are isolated or correlated with each other. The lower the ECC value, the lesser the correlation between antennas. The result of ECC is illustrated in Fig. 13, and the values can be derived from the following equation (4):

$$ECC_{ij} = \frac{|S_{ii}^* S_{ij} + S_{ji}^* S_{jj}|^2}{(1 - |S_{ii}|^2 - |S_{jj}|^2) \cdot (1 - |S_{jj}|^2 - |S_{ii}|^2)} \quad (4)$$

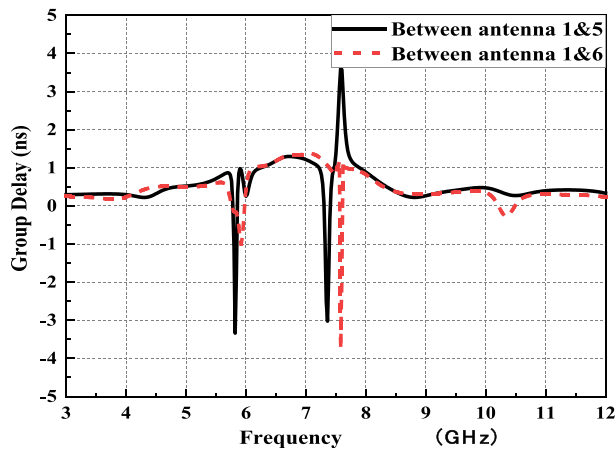


Figure 12. Group delay of the proposed antenna when positioned face to face.

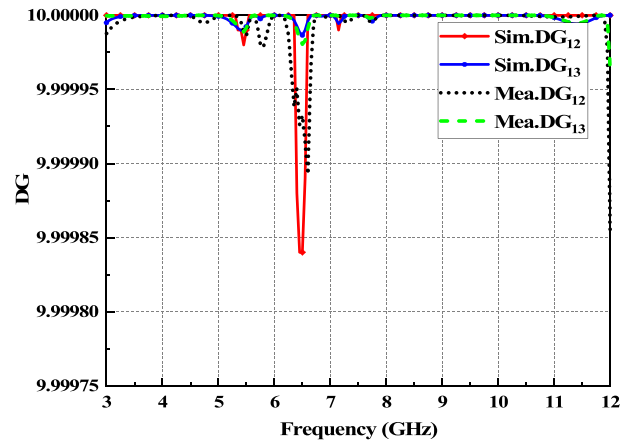


Figure 14. DG versus frequency for the proposed antenna.

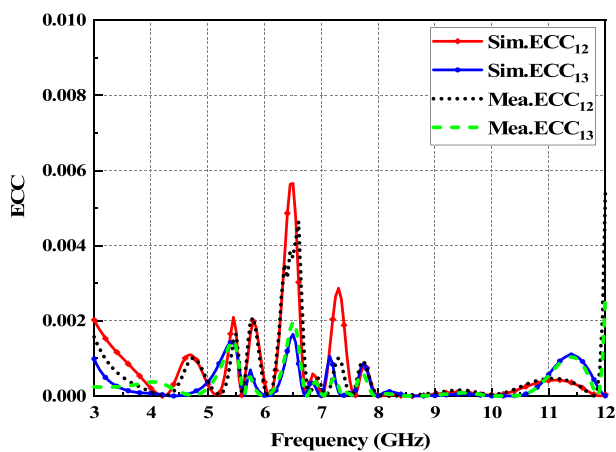


Figure 13. ECC versus frequency for the proposed antenna.

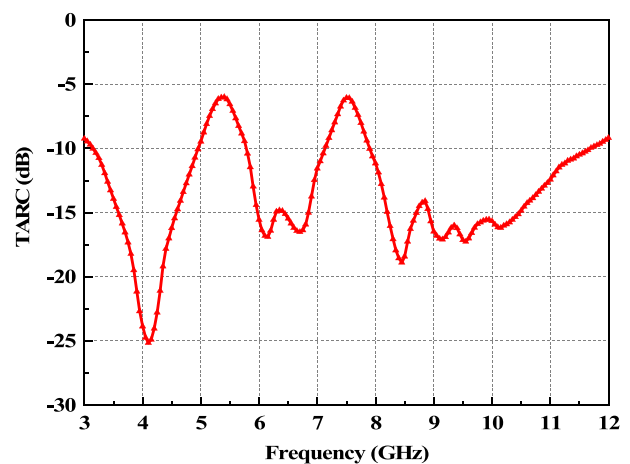


Figure 15. The results of the measured TARC.

**Diversity gain**

The DG is defined as the improvement in signal-to-noise (SNR) ratio from the combined signal from all the antennas of the diversity system relative to the SNR from a single antenna. The result of DG is illustrated in Fig. 14, and the values are calculated using the following equation (5):

$$DG_{ij} = 10\sqrt{1 - |ECC_{ij}|^2}. \tag{5}$$

**Total active reflection coefficient**

In a MIMO system, the mutual impedance between adjacent antennas and self-impedance of individual antenna elements are affected by antenna radiation. Therefore, analyzing only the individual S-parameter values of the antenna elements is insufficient. However, a new parameter called TARC can indicate changes in mutual impedance and self-impedance of array antennas, making it useful for investigating MIMO system properties. The TARC result is shown in Fig. 15, and the values can be computed using the following equation (6):

$$TARC = \frac{\sqrt{\sum_{i=1}^N \left( \sum_{j=1}^N S_{ij} \right)^2}}{\sqrt{N}}, \tag{6}$$

where  $N$  is the number of antenna elements and  $S_{ij}$  are the reflection coefficients between various ports of the MIMO antenna.

**Comparison with other already reported MIMO antennas**

A comparison between the proposed antenna and other similar antennas is shown in Table 2, which includes size, impedance bandwidth, isolation, ECC, and the number of notch bands. Compared to those previously reported, the proposed antenna is relatively small and achieves high isolation. It is worth noting that  $\lambda$  in Table 2 is the wavelength of the lowest operating frequency.

**Conclusion**

An ACS-fed MIMO antenna for UWB application with dual-band notch characteristics is designed and presented in this article. To achieve polarization diversity and better isolation among antenna elements, four antenna elements of the MIMO antenna are arranged in an orthogonal arrangement. The isolation is better than 18 dB for the proposed antenna system, although the elements are closely spaced. Besides, two L-shaped slots are etched on each radiating element to obtain dual-band (WLAN/X-satellite)

**Table 2.** Performance comparison of the proposed antenna with existing literature

Reference	Size in terms of wavelength	Impedance bandwidth (GHz)	Isolation (dB)	ECC	Number of notch bands
[20]	$0.51\lambda \times 0.51\lambda$	3.5–12.0	>15	<0.05	2
[21]	$0.43\lambda \times 0.47\lambda$	2.7–11.0	>18	<0.03	1
[22]	$0.24\lambda \times 0.35\lambda$	2.67–11.7	>15	<0.02	2
[23]	$0.44\lambda \times 0.44\lambda$	3.1–14.0	>18	<0.012	1
[24]	$0.67\lambda \times 0.81\lambda$	3.9–17.1	>10	<0.02	0
[25]	$0.4\lambda \times 0.4\lambda$	3.1–10.6	>25	<0.035	3
[26]	$0.33\lambda \times 0.33\lambda$	3.1–11.7	>14	<0.03	0
[27]	$0.69\lambda \times 0.69\lambda$	2.6–11.0	>17.4	<0.001	0
[28]	$0.38\lambda \times 0.38\lambda$	3.0–15.0	>15	<0.15	0
[29]	$0.43\lambda \times 0.43\lambda$	4.8–19.4	>15	<0.01	0
[30]	$0.33\lambda \times 0.33\lambda$	2.54–10.74	>10	<0.05	1
This work	$0.39\lambda \times 0.39\lambda$	3.4–12.2	>18	<0.006	2

suppression characteristics in the UWB range. The MIMO performance parameters of the proposed antenna are evaluated, proving acceptable performance in ECC, DG, and TARC.

**Funding statement.** This work was supported by the Anhui Provincial Natural Science Foundation (Grant No. 2108085MF200); the Natural Science Research Project of Anhui Educational Committee (Grant No. 2022AH051583); and the Graduate Innovation Fund of Anhui University of Science and Technology (Grant No. 2022CX2082).

**Competing interests.** The authors report no conflict of interest.

## References

- Li Q, Sun Y and Fang H (2021) Compact ACS-fed UWB MIMO antenna with dual band notches. *Applied Computational Electromagnetics Society Journal* **36**(1), 55–60.
- Ren W, Hu S-W and Jiang C (2016) An ACS-fed F-shaped monopole antenna for GPS/WLAN/WiMAX applications. *International Journal of Microwave and Wireless Technologies* **9**(5), 1123–1129.
- Naidu PV, Mahesh Babu D, Sai Haranadh A, Kumar S, Kumar A, Vummadisetty N and Pavansai D (2022) Design and performance analysis of 4-port trophy shaped MIMO antenna for tri-band applications. *Microsystem Technologies* **28**(4), 1037–1046.
- Wang W, Wu Y, Wang W and Yang Y (2021) Isolation enhancement in dual-band monopole antenna for 5G applications. *IEEE Transactions on Circuits and Systems II: Express Briefs* **68**(6), 1867–1871.
- Rajmohan R, Vishvaksean KS and Kalidoss R (2021) Compact four port slot based MIMO antenna with isolation enhancement. *International Journal of Electronics* **108**(7), 1075–1088.
- Chandel R, Gautam AK and Rambabu K (2018) Design and packaging of an eye-shaped multiple-input–multiple-output antenna with high isolation for wireless UWB applications. *IEEE Transactions on Components, Packaging and Manufacturing Technology* **8**(4), 635–642.
- Luo C-M, Hong J-S and Zhong -L-L (2015) Isolation enhancement of a very compact UWB-MIMO slot antenna with two defected ground structures. *IEEE Antennas and Wireless Propagation Letters* **14**, 1766–1769.
- Zhang S and Pedersen GF (2016) Mutual coupling reduction for UWB MIMO antennas with a wideband neutralization line. *IEEE Antennas and Wireless Propagation Letters* **15**, 166–169.
- Wang Z, Mu W, Yang M and Li C (2022) Design of compact multi-band MIMO antenna based on ground neutralization line decoupling. *The Applied Computational Electromagnetics Society Journal (ACES)* **37**(6), 702–715.
- Liu F, Guo J, Zhao L, Huang G-L, Li Y and Yin Y (2020) Dual-band metasurface-based decoupling method for two closely packed dual-band antennas. *IEEE Transactions on Antennas and Propagation* **68**(1), 552–557.
- Wang L, Du Z, Yang H, Ma R, Zhao Y, Cui X and Xi X (2019) Compact UWB MIMO antenna with high isolation using fence-type decoupling structure. *IEEE Antennas and Wireless Propagation Letters* **18**(8), 1641–1645.
- Lin G-S, Sung C-H, Chen J-L, Chen L-S and Houng M-P (2017) Isolation improvement in UWB MIMO antenna system using carbon black film. *IEEE Antennas and Wireless Propagation Letters* **16**, 222–225.
- Zhou Z, Liu S, Li W, An T and Hu Z (2021) A wideband MIMO antenna with high isolation for 5G application. *International Journal of RF and Microwave Computer-Aided Engineering* **32**(3), 1–10.
- Chandel R, Gautam AK and Rambabu K (2018) Tapered fed compact UWB MIMO-diversity antenna with dual band-notched characteristics. *IEEE Transactions on Antennas and Propagation* **66**(4), 1677–1684.
- Liu L, Cheung SW and Yuk TI (2015) Compact MIMO antenna for portable UWB applications with band-notched characteristic. *IEEE Transactions on Antennas and Propagation* **63**(5), 1917–1924.
- Kapure VR and Rathod SS (2023) A two element EBG-inspired UWB MIMO antenna with triple band notched characteristics and high isolation. *Sādhanā* **48**(1), 1–16.
- Chakraborty M, Pal S and Chattoraj N (2019) Quad notch UWB antenna using combination of slots and split-ring resonator. *International Journal of RF and Microwave Computer-Aided Engineering* **30**(3), 1–10.
- You X, Du C-Z and Yang Z-P (2023) A flexible CPW 2-port dual notched-band UWB-MIMO antenna for wearable IoT applications. *Progress In Electromagnetics Research C* **128**, 155–168.
- Yang M and Zhou J (2020) A compact pattern diversity MIMO antenna with enhanced bandwidth and high-isolation characteristics for WLAN/5G/WiFi applications. *Microwave and Optical Technology Letters* **62**(6), 2353–2364.
- Sri GR, Rani AJ and Saritha V (2020) Design and implementation of a very compact MIMO antenna providing dual notches at WLAN and X-band. *Progress in Electromagnetics Research C* **104**, 241–252.
- Ibrahim AA and Ali WAE (2021) High isolation 4-element ACS-fed MIMO antenna with band notched feature for UWB communications. *International Journal of Microwave and Wireless Technologies* **14**(1), 54–64.
- Kaur H, Singh HS and Upadhyay R (2022) Design of a compact quasi-self-complementary UWB-MIMO antenna with dual band-notched characteristics for wireless communication applications. *International Journal of Electronics* **110**(5), 804–828.
- Suresh AC and Reddy TS (2022) A flower shaped miniaturized 4x4 MIMO antenna for UWB applications using characteristic mode analysis. *Progress in Electromagnetics Research C* **119**, 219–233.



24. **Desai A, Kulkarni J, Kamruzzaman MM, Hubalovsky S, Hsu H-T and Ibrahim AA** (2022) Interconnected CPW fed flexible 4-port MIMO antenna for UWB, X, and Ku band applications. *IEEE Access* **10**, 57641–57654.
25. **Agarwal M, Dhanoa JK and Khandelwal MK** (2020) Ultrawide band two-port MIMO diversity antenna with triple notch bands, stable gain and suppressed mutual coupling. *AEU – International Journal of Electronics and Communications* **120**, 153225.
26. **Kaur H, Singh HS and Upadhyay R** (2022) Design and analysis of compact quad-element MIMO antenna with asymmetrical ground structures for ultra-wideband communication. *Wireless Personal Communications* **124**(4), 3105–3127.
27. **Naktong W and Ruengwaree A** (2020) Four-port rectangular monopole antenna for UWB-MIMO. *Progress in Electromagnetics Research B* **87**, 19–38.
28. **Sipal D, Abegaonkar MP and Koul SK** (2017) Easily extendable compact planar UWB MIMO antenna array. *IEEE Antennas and Wireless Propagation Letters* **16**, 2328–2331.
29. **Singhal S** (2019) Four element ultra-wideband fractal multiple-input multiple-output antenna. *Microwave and Optical Technology Letters* **61**(12), 2811–2818.
30. **Kaur H, Singh HS and Upadhyay R** (2023) Design and analysis of planar four-port UWB-MIMO antenna with band-rejection capability. *International Journal of Microwave and Wireless Technologies*, 1–13.



**Zhongyuan Lu** received the B.E degree from Hefei University of Economics in 2020. He is currently pursuing M.S. degree in Anhui University of Science and Technology. His current research interest includes the theory and design of MIMO antenna.



**Han Lin** is a Lecturer at Anhui University of Science and Technology. She received the Ph.D. degree in Electromagnetic Field and Microwave Technique from the Nanjing University of Aeronautics and Astronautics, Nanjing, P.R. China, in 2015. Her research interests include computational electromagnetic methods, antenna theory and design.



**Zhonggen Wang** received the PhD degree in electromagnetic field and microwave technique from the Anhui University of China (AHU), Hefei, P.R. China, in 2014. Since 2014, he has been with the School of Electrical and Information Engineering, Anhui University of Science and Technology. His research interests include computational electromagnetics, array antennas, and reflect arrays.



**Wenyan Nie** is a professor at Huainan Normal University. She received her B.S. and M.S. degrees from Anhui University of Science and Technology in 2007 and 2012, respectively. Her research interests include computational electromagnetic methods, antenna theory and design.



**Weidong Mu** received the B.E. degree from Anhui University of Science and Technology in 2020. He is currently pursuing the M.S. degree in Anhui University of Science and Technology. His current research interest includes the theory and design of MIMO antenna.